



# **Comparison of the High-Temperature Oxidation Behavior of Subsolvus and Supersolvus Treated Advanced Powder Metallurgy Disk Alloys**

Chantal K. Sudbrack, Tim P. Gabb and David R. Hull  
**NASA Glenn Research Center**

Jonathan D Yu  
**Stanford University**

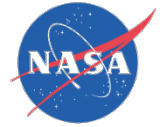
Timothy T Gorman  
**University of Dayton**

*Acknowledgements: James Smialek, Jack Telesman, Sue Draper, Mike Nathal for valuable discussions (NASA-GRC); Analytical Science Group for experimental support (NASA-GRC); GE Engines and Honeywell International for providing samples*

*Funding: NASA's Aviation Safety and Fundamental Aeronautics Programs*

---

*March 6, 2012*



## Background

- The drive in aerospace propulsion applications towards higher turbine inlet temperatures, which should improve engine efficiency, is leading to higher disk rim temperatures.

Currently at 650 °C → Long-range goal of 800 °C

- Advanced powder metallurgy (P/M) **nickel based superalloys** have been developed by industry, AFRL and NASA to address the properties needed at these elevated temperatures e.g. **Alloy 10**, LSHR, **ME3 (R104)**, RR1000
- It is well-established that oxidation can reduce fatigue life in disk alloys above 650°C by accelerated crack initiation and growth at defects, however it is not well-studied yet in disk alloys at 650 °C - 800°C **Protective coatings?**

Turbine stage  
schematic

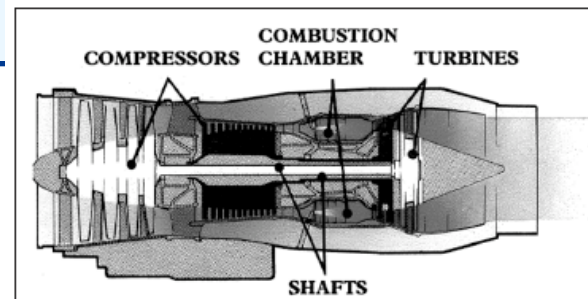
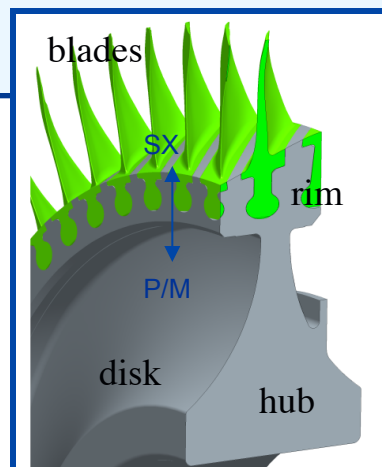
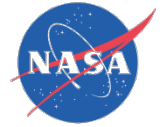


Figure 1. A schematic illustrating a cross section of a gas turbine engine.

*JOM, 51:1 (1999) 14-17.*

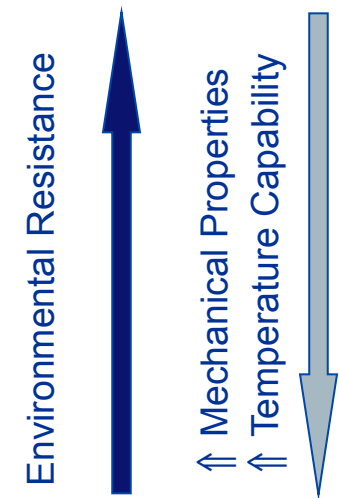


# Oxidation of Disk Alloys

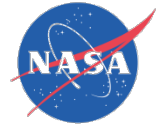
- Newer P/M disk alloys have substituted environmental resistance (Al, Cr levels) for strength (Mo, W, Ta, etc.)

High Cr  
Low Al  
  
**Cr<sub>2</sub>O<sub>3</sub>  
formers**

Disk Alloys wt. %	Cr	Al	Cr+Al	Cr/Al	Ti
Inconel 718	19.0	0.5	19.5	38	0.9
Waspaloy	19.5	1.3	20.8	15.6	3.0
Udimet 720	18.0	2.5	20.5	7.2	2.5
RR1000	14.6	3.0	17.6	5.0	3.6
<b>ME3</b>	<b>13.0</b>	<b>3.4</b>	<b>16.4</b>	<b>3.9</b>	<b>3.8</b>
<b>Alloy 10</b>	11.5	3.5	15.0	3.3	3.5



- Stable, slow growth of **protective Cr<sub>2</sub>O<sub>3</sub> external** scale with Al<sub>2</sub>O<sub>3</sub> subscale by internal oxidation with fast growth **deleterious TiO<sub>2</sub> scale**
  - Cast-wrought disk alloy comparison shows Ti content is rate controlling
- Mass change data suggests **classic parabolic growth (time<sup>1/2</sup>)** consistent with high temperature oxidation of Ni alloys for the **external oxide scale**
- Simplified models also predict **the penetration depth of the internal oxide by precipitation** to be proportional to **(time<sup>1/2</sup>)**



**Motivation:** Environmental attack has the potential to limit turbine disk durability, particularly in next generation engines which will run hotter.

**Understand environmental attack and its effect on the fatigue resistance of disk alloys**

### Approach:

- NASA research contracts with GE and Honeywell to identify coatings with good corrosion resistance. **In-house work now underway**
- Walk before run: oxidation is ubiquitous
- Supersolvus ME3 from GE
- Subsolvus Alloy10 from Honeywell

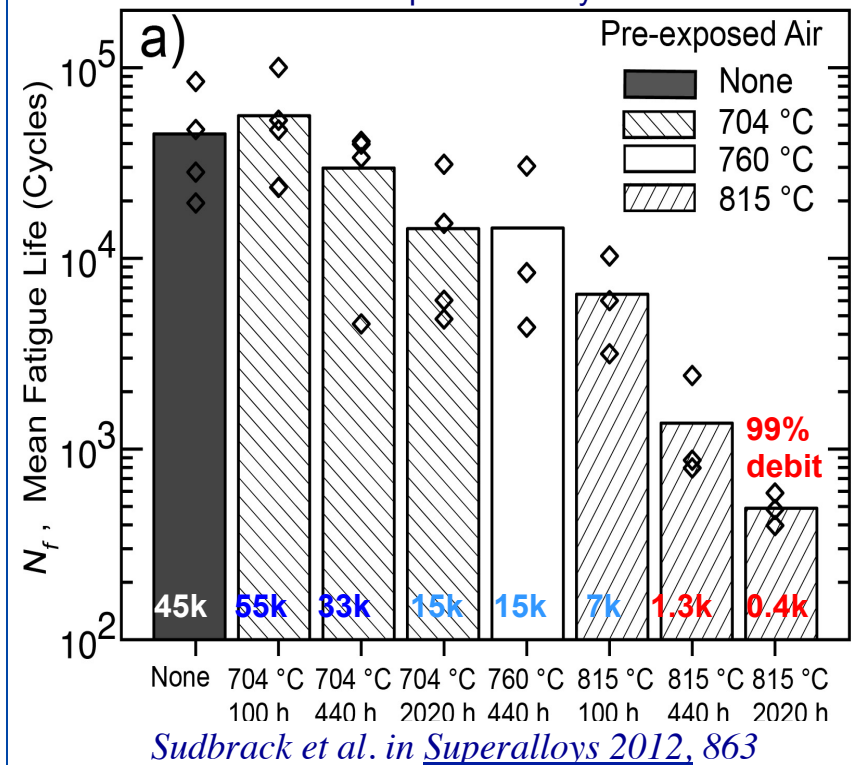
• **Flat coupon exposures in air: 704 °C, 760 °C and 815 °C up to 2,020 hours**

- NASA progress on fatigue response published in [Superalloys 2012](#)

### Notched LCF testing at 704 °C

$\sigma_{\max}=855$  MPa,  $R(\sigma)=0.05, 0.333$  Hz

Each test is represented by a diamond



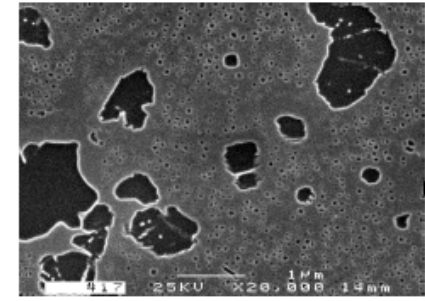
*Dwell Notched LCF: Telesman et al. in [Superalloys 2012](#), 853.*



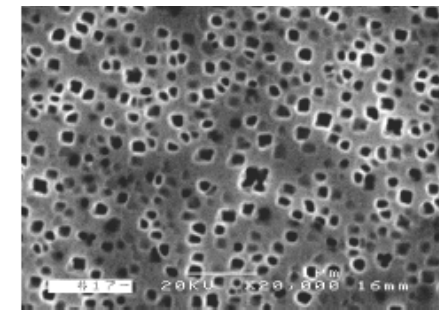


## Both fine grained and coarse grained disks are in flight

A fine grain size provides superior yield, tensile and low cycle fatigue strength → **Subsolvus heat treated**

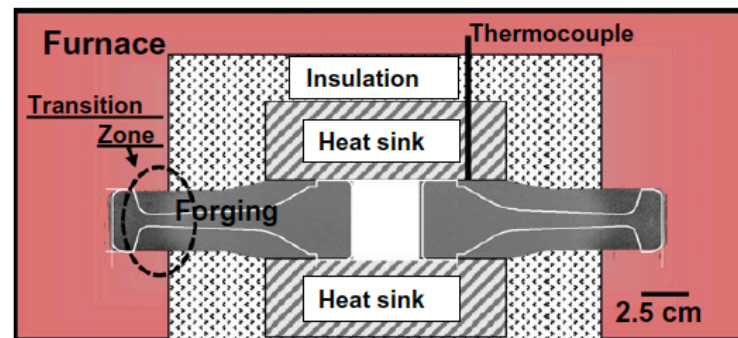


A coarse grain size provides superior creep and crack growth resistance → **Supersolvus heat treated**



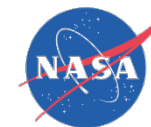
Dual-structure processing techniques to produce a fine grain bore in combination with a coarse grain web and rim offer significant benefits for advanced engine designs

Dual microstructure heat treatment (DMHT) technology



*J. Gayda et al. in Superalloys 2004, 323*

Fig. 1. Schematic of dual microstructure heat treatment (DMHT) assembly used for solution heat treatment of disk, with location of grain size transition zone indicated.



## As-processed microstructure prior to exposures

wt.%	Cr	Co	Al	Ti	Nb	Ta	Mo	W	C	B	trace	Ni
<b>ME3</b>	13	21	3.4	3.7	0.8	2.4	3.8	2.1	0.05	0.02	Si, Fe, N, O, S, Zr	49.6
<b>Alloy 10</b>	12	19	3.4	3.5	1.4	1.4	2.5	4.6	0.03	0.03	0.06 Zr	bal

### Supersolvus ME3

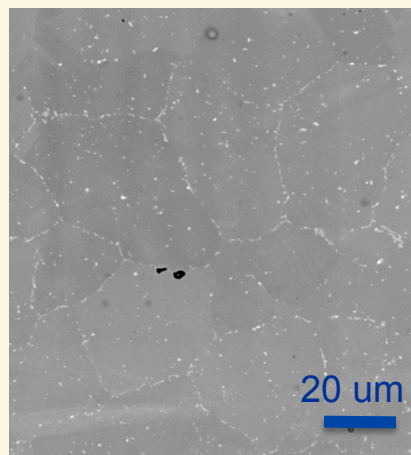
Grain size: 25  $\mu\text{m}$  – 34  $\mu\text{m}$

Cr-rich  $\text{M}_{23}\text{C}_6$

- carbides ornament GBs

Ti,Ta,Nb-rich MC

- carbides in interior & GBs

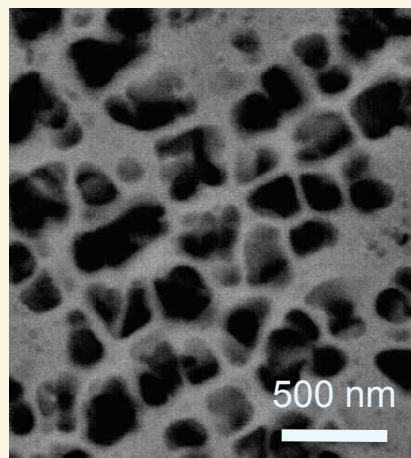


Volume Fraction: 0.55

Primary  $\gamma'$ : None

Secondary  $\gamma'$ : 190 – 330 nm

Tertiary  $\gamma'$ , 18 – 39 nm



### Subsolvus A10

GS: 5.26  $\pm$  0.28  $\mu\text{m}$  (95%CI)

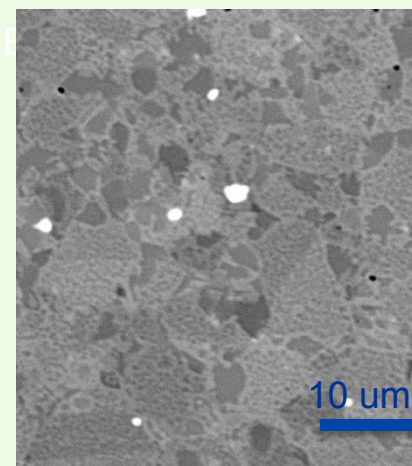
Micron sized  $\text{W}_3\text{B}_2$

Cr-rich  $\text{M}_{23}\text{C}_6$

- carbides ornament GBs

Ti,Ta,Nb-rich MC

- carbides in interior & GBs

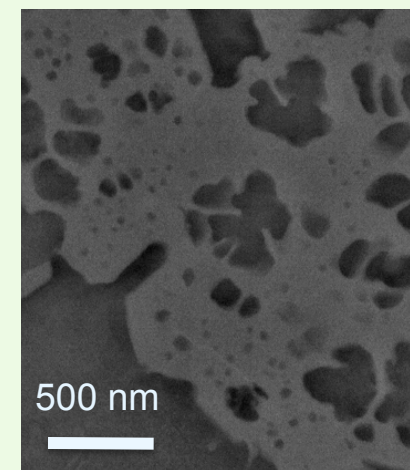


Volume Fraction: 0.57

Primary  $\gamma'$ :  $\sim$  2 – 5  $\mu\text{m}$

Secondary  $\gamma'$ :  $\sim$  100-500 nm

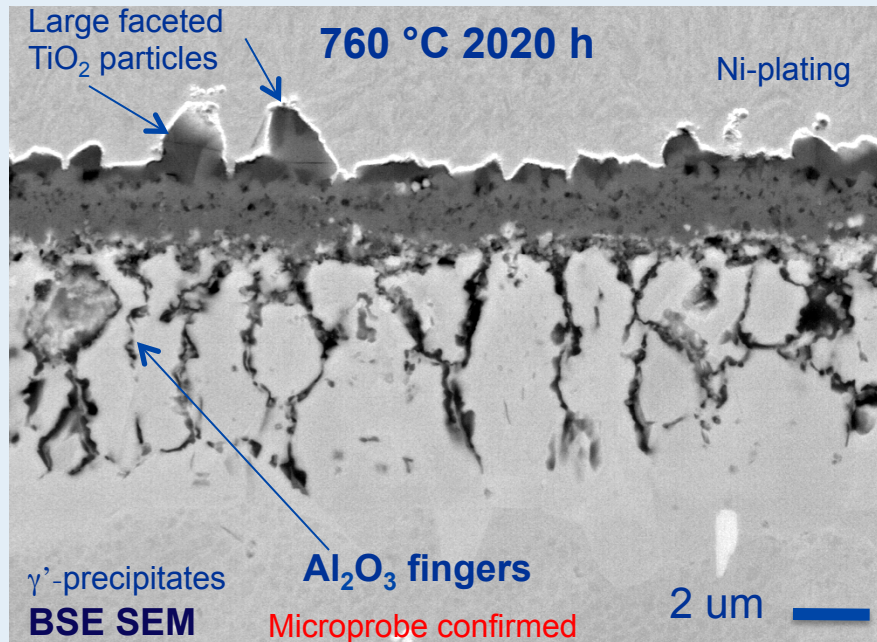
Tertiary  $\gamma'$ ,  $\sim$  20 – 40 nm



$\gamma'$  ( $\text{L1}_2$ ): Al, Ti partitioning,  $\gamma$  (fcc): Cr, Co, Mo partitioning

# How these disk alloys oxidize

## Supersolvus ME3



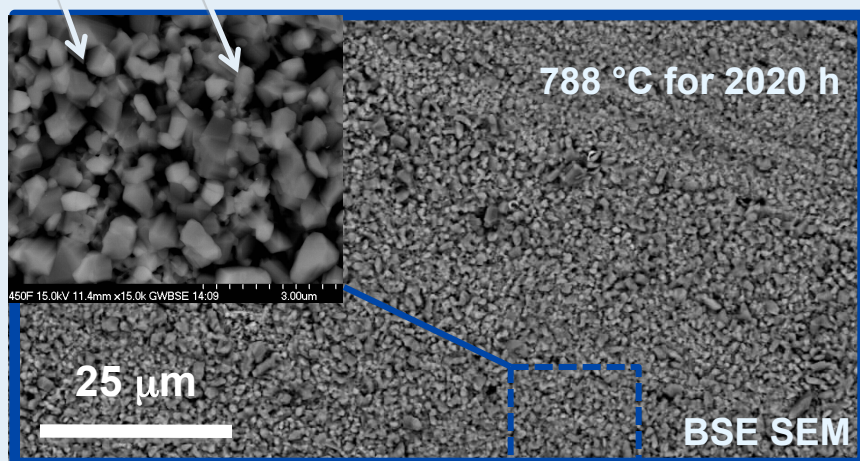
X-Ray Diffraction confirmed

$\text{Cr}_2\text{O}_3 + \text{TiO}_2$

$\gamma'$ -precipitate dissolution layer

- $\text{Cr}_2\text{O}_3$  external scale is intermixed with  $\text{TiO}_2$  grains
- Ti is driven towards the surface to form primarily superficial  $\text{TiO}_2$  grains
- Branched  $\text{Al}_2\text{O}_3$  forms an internal oxide underneath the external scale causing  $\gamma'$ -precipitates to dissolve in the near surface region

## Plan view



From cross sections, track evolution of

1.  $\text{Cr}_2\text{O}_3$ - $\text{TiO}_2$  external scale thickness
2.  $\text{Al}_2\text{O}_3$  finger penetration depth
3.  $\gamma'$ -precipitate dissolution layer thickness

Simple Power Law Fit

$k$  is the rate constant

$$y = (k \cdot t)^n$$

$n$  is the temporal exponent

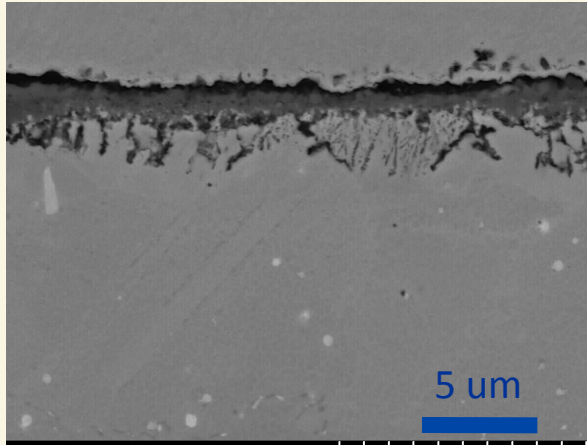


# Track layer thicknesses precisely

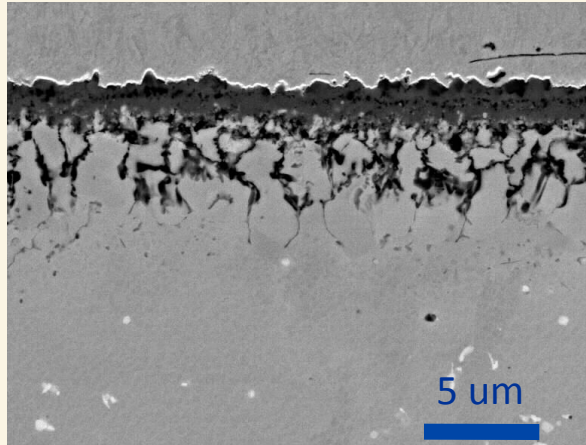


## Supersolvus ME3

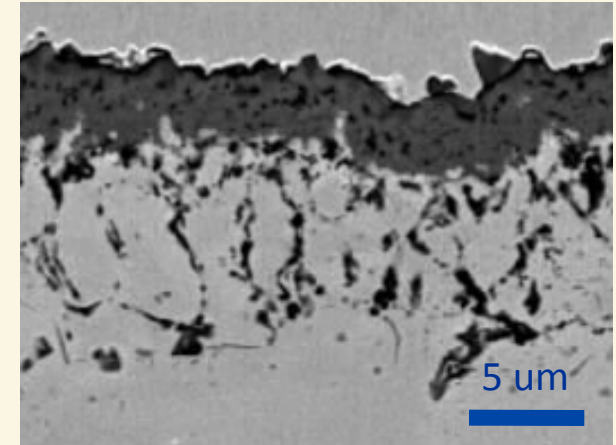
704 °C for 2020 h



760 °C for 2020 h



815 °C for 2020 h



### Three Areas

→ SEM, DIC

1. Avg. Oxide Scale Thickness ( $\mu\text{m}$ )

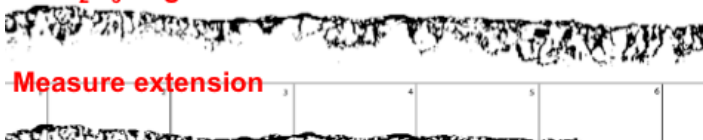
2. Avg.  $\text{Al}_2\text{O}_3$  Finger Depth ( $\mu\text{m}$ )

Binary selection



ID Scale (measure thickness @ every value across )

ID  $\text{Al}_2\text{O}_3$  fingers

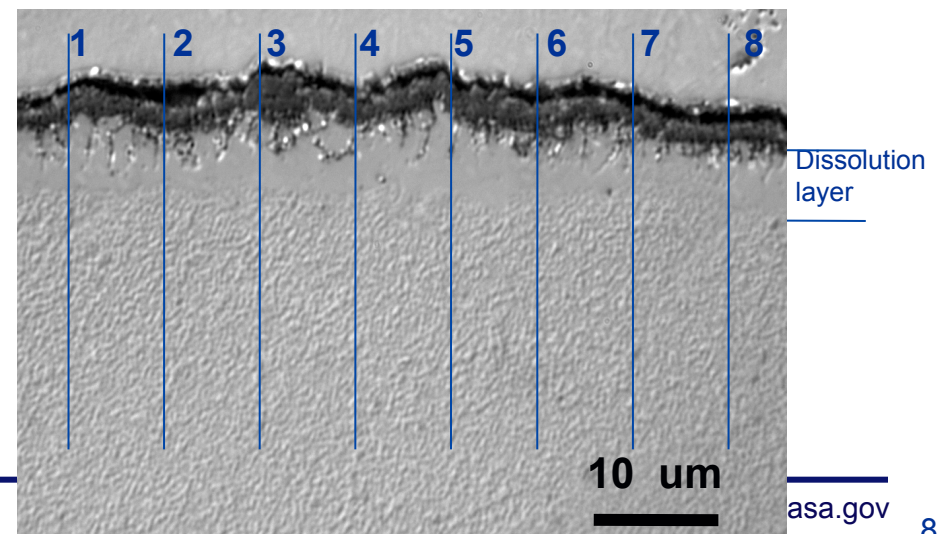


Measure extension



3. Avg.  $\gamma'$ -dissolution layer thickness ( $\mu\text{m}$ )

Differential Interference Contrast: 815 °C for 440 h

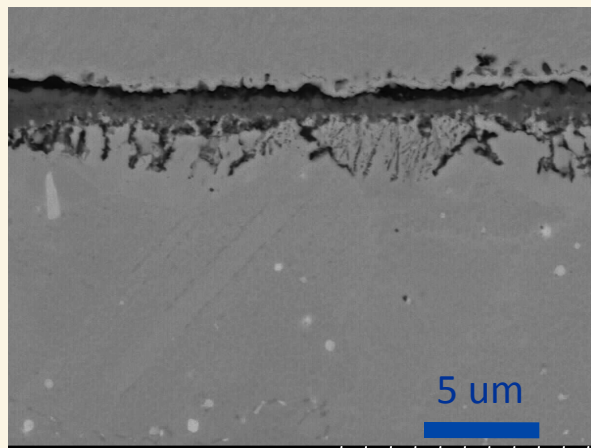


# Track layer thicknesses precisely

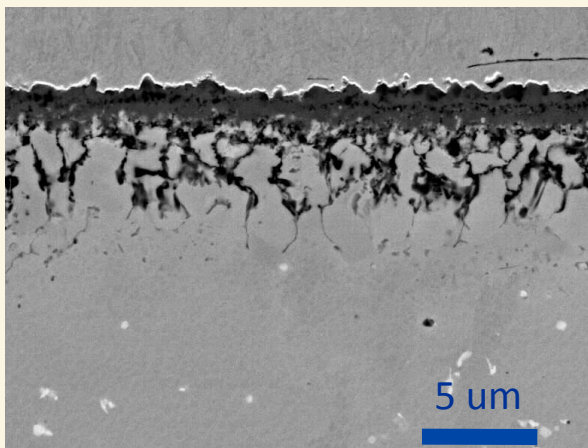


## Supersolvus ME3

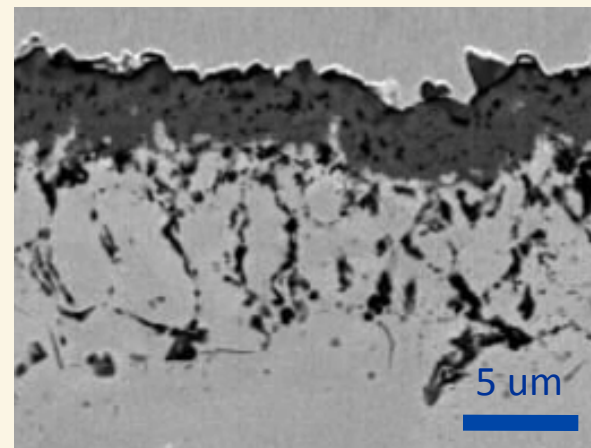
704 °C for 2020 h



760 °C for 2020 h

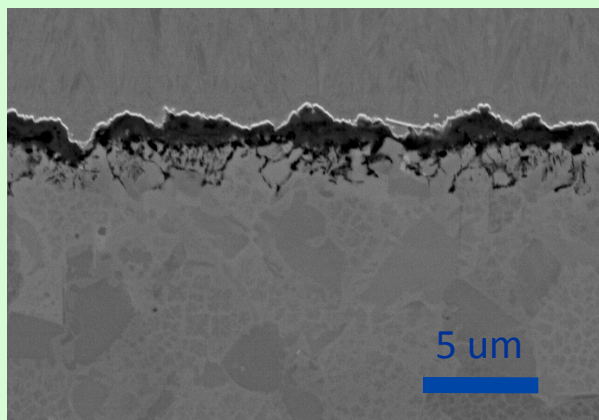


815 °C for 2020 h

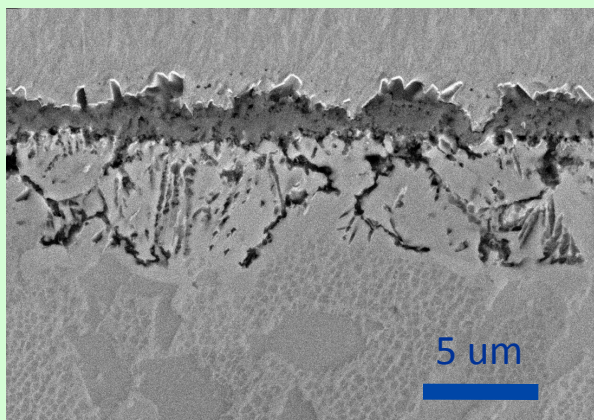


## Subsolvus A10

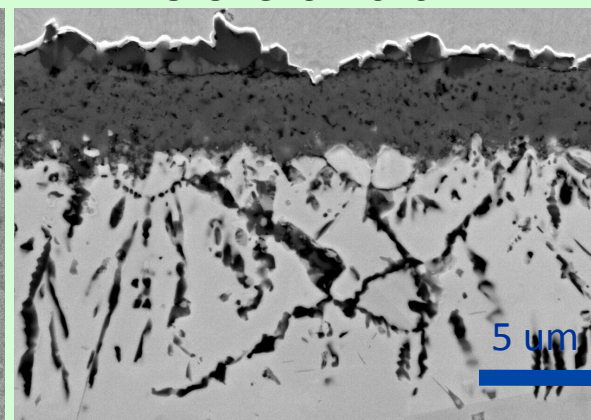
704 °C for 2020 h

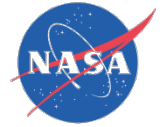


760 °C for 2020 h



815 °C for 2020 h





## 2020 h end points for three isotherms

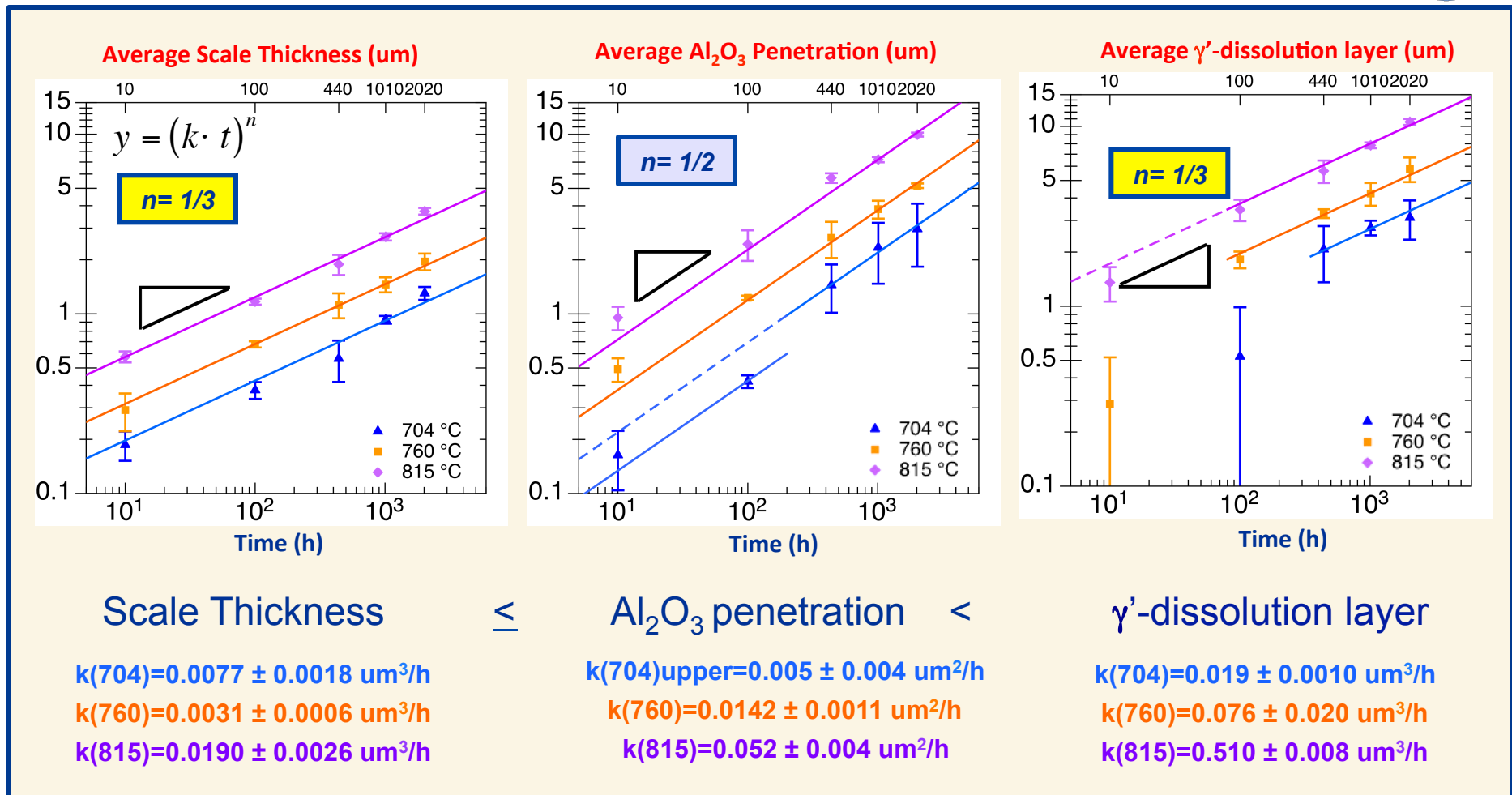
<b>Supersolvus ME3</b>	<b>Scale Thickness (<math>\mu\text{m}</math>)</b>	<b>Alumina Penetration Depth (<math>\mu\text{m}</math>)</b>	<b><math>\gamma'</math>-Dissolution Layer (<math>\mu\text{m}</math>)</b>
Technique	SEM (3840)	SEM (24)	DIC (24)
Distributed	Log normal	Normal	Normal
704°C	$1.32 \pm 0.61$	$2.88 \pm 0.81$	$3.14 \pm 1.01$
760°C	$1.97 \pm 0.67$	$5.23 \pm 0.67$	$5.96 \pm 1.20$
815°C	$3.79 \pm 1.57$	$10.00 \pm 1.16$	$10.75 \pm 1.13$

	<b>Subsolvus A10</b>	<b>Scale Thickness (<math>\mu\text{m}</math>)</b>	<b>Alumina Penetration Depth (<math>\mu\text{m}</math>)</b>	<b><math>\gamma'</math>-Dissolution Layer (<math>\mu\text{m}</math>)</b>
	Technique	SEM (3840)	SEM (24)	DIC (24)
	Distributed	Log normal	Normal	Normal
slower	704°C	$0.69 \pm 0.22$	$1.32 \pm 0.38$	—
	760°C	$1.77 \pm 0.14$	$3.97 \pm 0.66$	$5.80 \pm 1.26$
compar- able	815°C	$4.17 \pm 0.32$	$9.43 \pm 0.82$	$12.76 \pm 0.60$

*How do the reaction kinetics compare?*



## Supersolvus ME3

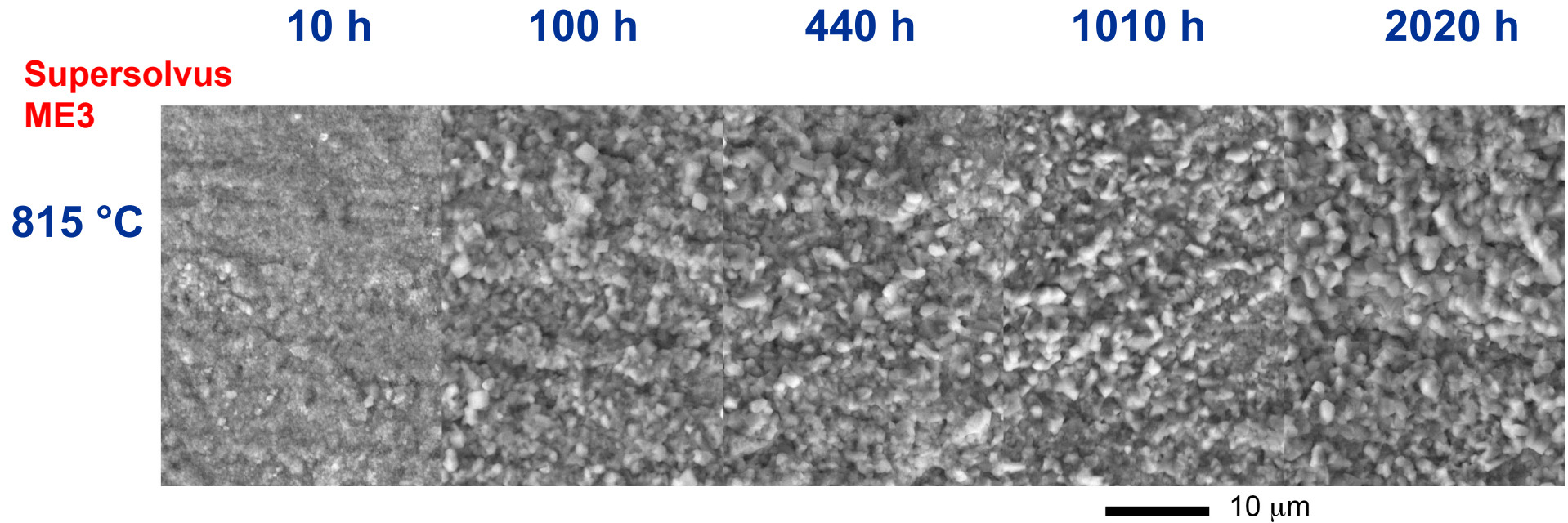


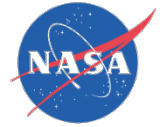
- Branched  $\text{Al}_2\text{O}_3$  penetration depth follows parabolic growth law
- Both external scale thickness and  $\gamma'$ -dissolution layer follow a cubic growth law
  - $\gamma'$ -dissolution layer is three times thicker than external oxide scale



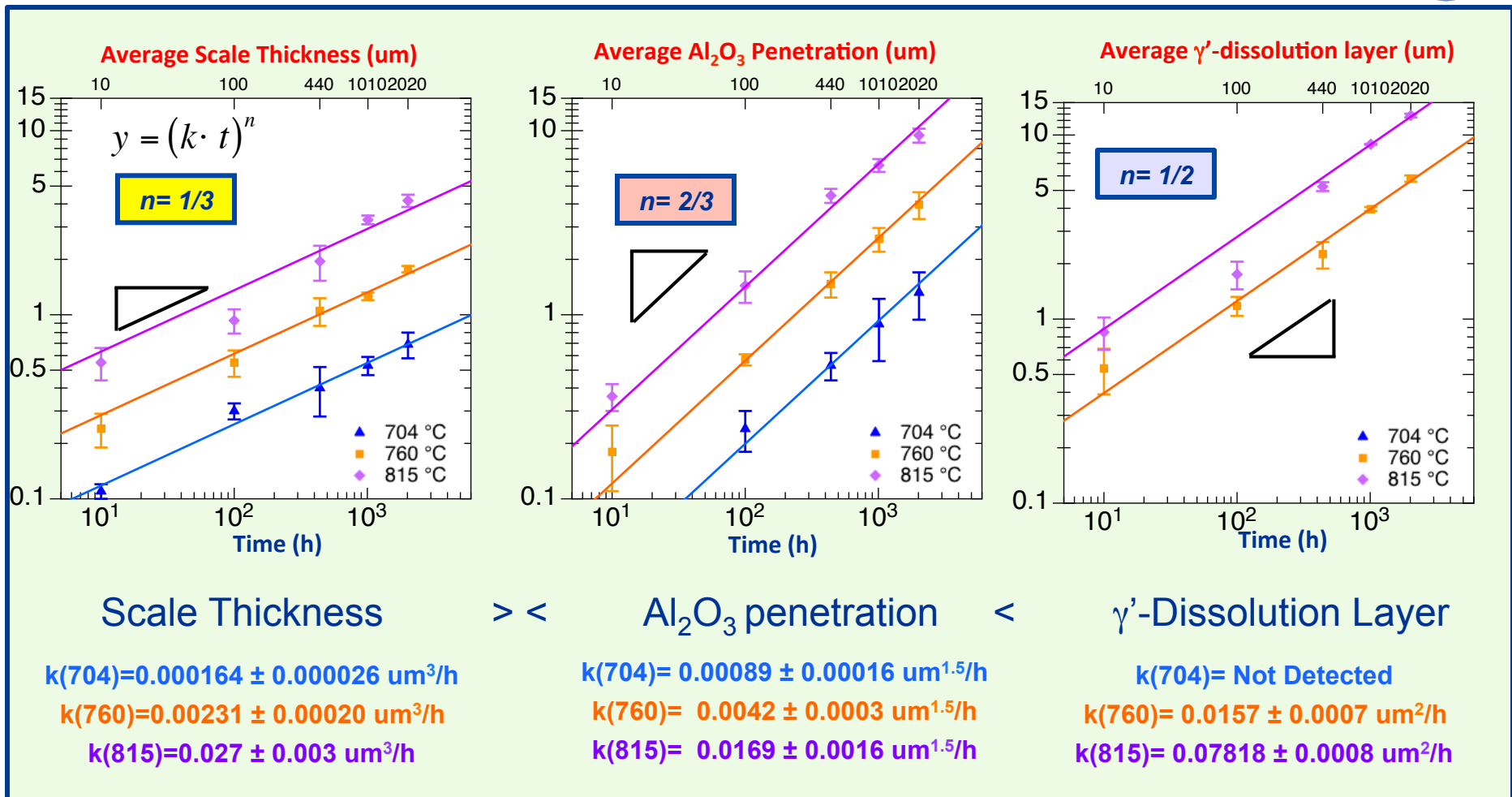


## Grain growth in external oxide may be responsible for $t^{1/3}$ kinetics





## Subsolvus A10

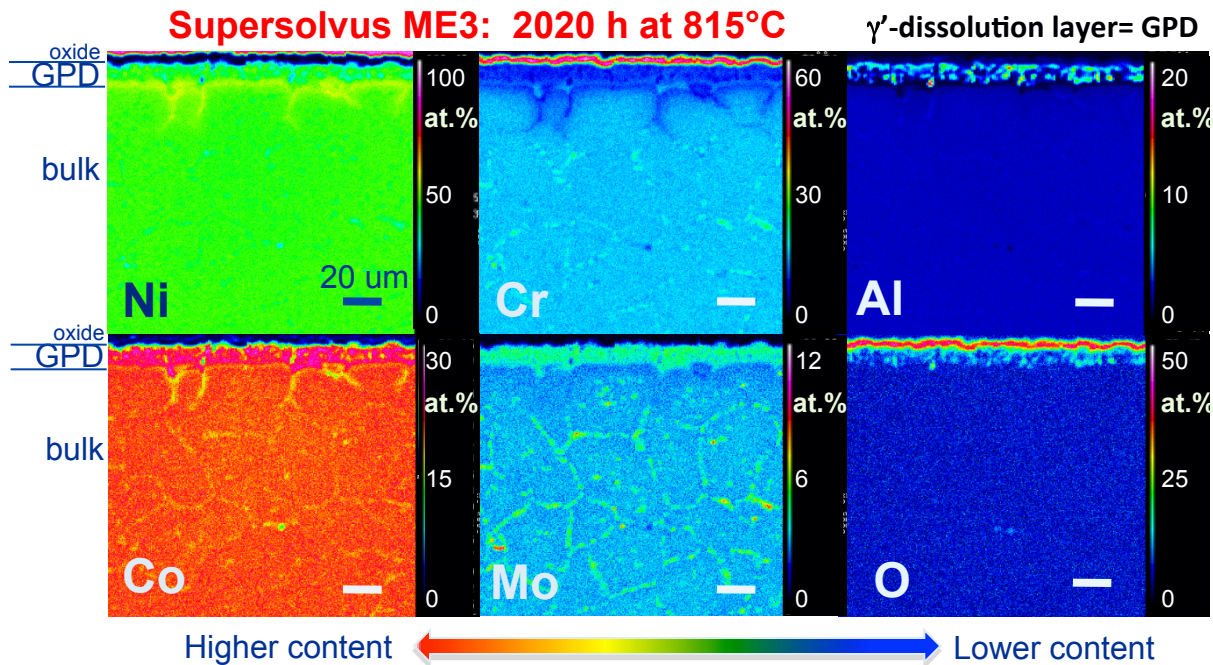


**Agreement:** External scale thickness shows a cubic growth law

**Difference:**  $\text{Al}_2\text{O}_3$  penetration depth shows larger temporal exponent  $\rightarrow$  Primary  $\gamma'$ -ppts.

**Difference:**  $\gamma'$ -dissolution layer evolves parabolically  $\rightarrow$  short circuit diffusion

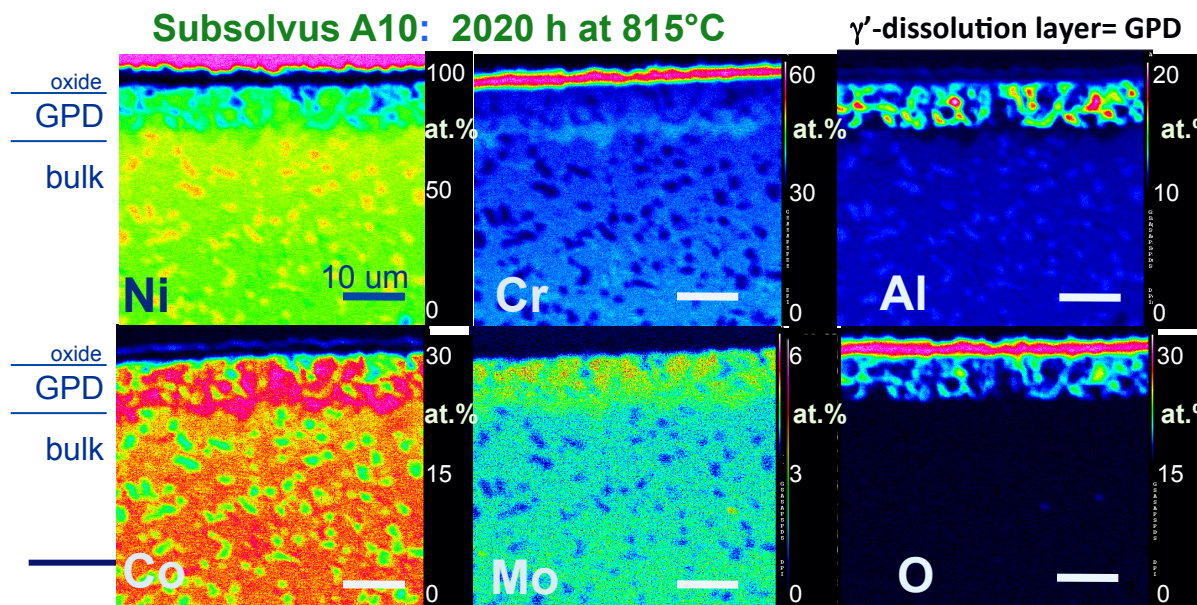
# Microprobe chemical mapping: insight into diffusional processes



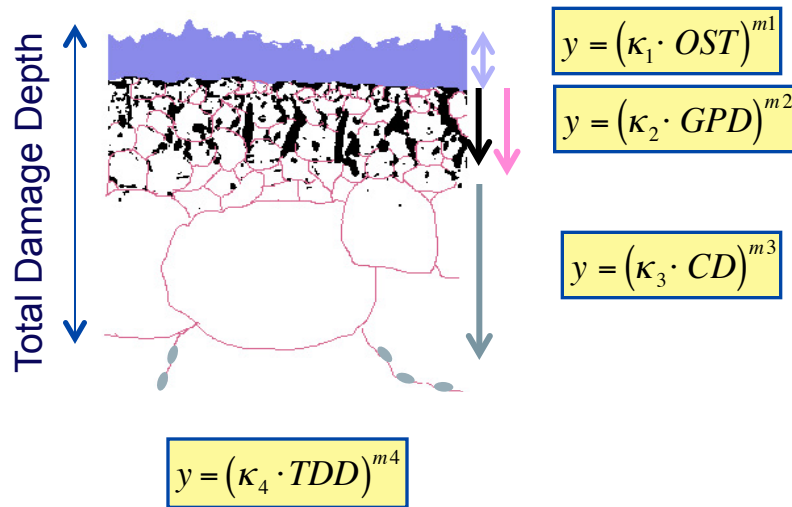
wt.%	Cr	Co	Al	Mo	C
<b>ME3</b>	<b>13</b>	<b>21</b>	<b>3.4</b>	<b>3.8</b>	<b>0.05</b>
<b>Alloy 10</b>	<b>12</b>	<b>19</b>	<b>3.4</b>	<b>2.5</b>	<b>0.03</b>

- GPD: Depletion of the major oxide elements Ti, Al, Cr, Ta
- GPD is  $\gamma$ -like, enriched in Co, Mo, but not Cr
- Partitioning in primary  $\gamma'$
- Interfacial volume between GPD and bulk enriched in Cr and Ti
 

$D(\text{Al}) \approx 3 D(\text{Cr})$
- A striking feature is the dissolution of coarsened  $(\text{Cr}, \text{Mo})_{23}\text{C}_6$  carbides past the GPD
  - Associated GBs are depleted in Cr, Mo and Co
- More analysis planned!



# Precise layer measurements give predictive capability for fatigue life models

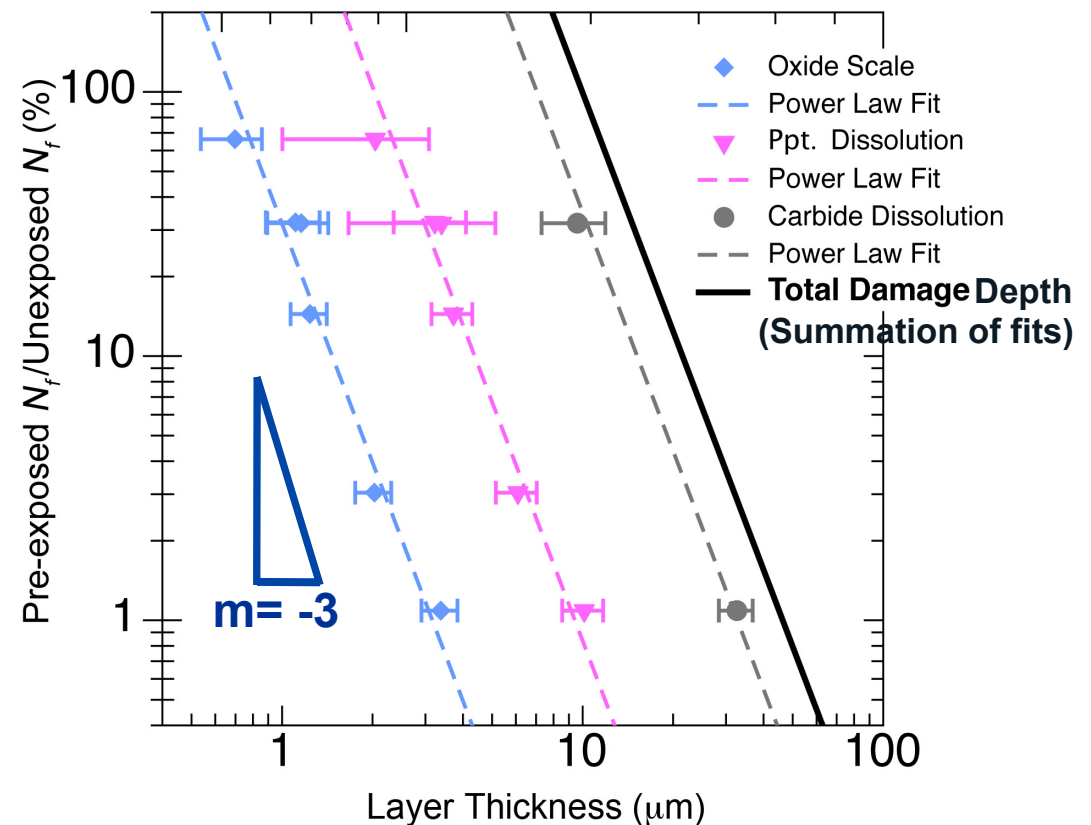


*By substitution*

$$y = \left( \kappa_n \cdot (k_n(T) \cdot t)^{1/3} \right)^{-3} \propto t^{-1}$$

**Supersolvus ME3:** Notched LCF data at 704 °C

*Sudbrack et al. in Superalloys 2012, 863*



**Future work** → characterization of fatigue response for subsolvus Alloy 10





# Conclusions

- For isothermal static oxidation of such alloys at 704 °C, 760 °C, and 815 °C, **fine-grained subsolvus disks oxidize similarly to coarse-grained supersolvus disks** despite their differences in alloy chemistry and microstructure:
  - Oxidation by-products: A continuous  $\text{Cr}_2\text{O}_3$  external scale forms with superficial, faceted  $\text{TiO}_2$  grains primarily at the exposed surface with an internal subscale of branched  $\text{Al}_2\text{O}_3$  extends into a layer where the  $\gamma'$ -precipitates are dissolved.
  - External oxide growth: Sustained partially by dissolution of Cr-rich  $\text{M}_{23}\text{C}_6$  grain boundary carbides, it has a **cubic growth** likely due to non-negligible oxide grain growth.
- However, the fine-grained subsolvus disks with primary  $\gamma'$ -precipitates can respond differently than coarse-grained supersolvus for:
  - Internal oxide growth: Larger temporal exponent for penetration depth of  $(\text{time})^{2/3}$  for subsolvus compared to  $(\text{time})^{1/2}$  for supersolvus
  - $\gamma'$ -dissolution layer growth: Larger temporal exponent of  $(\text{time})^{1/2}$  compared to  $(\text{time})^{1/3}$
- Interestingly, over certain temperature exposures, the penetration depth of the internal oxide could be smaller for the subsolvus than supersolvus, suggesting that in addition to coarse  $\gamma'$ -precipitates other factors influence the growth process
  - Additional experiments: subsolvus ME3 and supersolvus Alloy 10